Photoinduced non-linear optical effects in lanthanum calcium borate single crystals

ALI H. RESHAK, S. AULUCK
Physics Department, Indian Institute of Technology, Roorkee (Uttaranchal) 247667, India

I. V. KITYK*
Institute of Physics, J. Dlugosz Academy of Czestochowa, Al. Armii Krajowej 13/15, Czestochowa, Poland
E-mail: i.kityk@mp.ajd.czest.pl

A. MAJCHROWSKI
Institute of Applied Physics Military University of Technology, 2 Kaliskiego Str., 00-908 Warsaw, Poland

D. KASPROWICZ, M. DROZDOWSKI
Faculty of Technical Physics, Poznan University of Technology, Nieszawska 13 A, 60 - 965 Poznan, Poland

J. KISIELEWSKI, T. LUKASIEWICZ
Institute of Electronic Materials Technology, 133 Wolczanska Str., 01-919 Warsaw, Poland

E. MICHALSKI
Institute of Applied Physics Military University of Technology, 2 Kaliskiego Str., 00-908 Warsaw, Poland

Published online: 17 February 2006

We have revealed that lanthanum calcium borate ($La_2CaB_{10}O_{19}$) crystals show two-photon absorption (TPA) favored by UV laser field. UV-induced TPA measurements were performed under illumination of a Xe-F laser ($\lambda = 217$nm) as a photoinducing (pumping) beam. This pumping laser beam created a thin surface layer (about 85 nm) that was a source of the observed photoinduced TPA. Use of the longer photoinducing wavelength leads to a substantial decrease of the photoinduced TPA. The performed DFT calculations of the band energy dispersion clearly show that the effect observed is due to specific band energy dispersion between the sub-bands. The Raman shifted Nd-YAG laser radiation ($\lambda = 1.9$ μm) as well as its second and fourth harmonics ($\lambda = 950$ and $\lambda = 475$ nm, respectively) were used as fundamental (probing) beams of the TPA. The highest values of the TPA β coefficient were achieved for polarization of the pumping light directed along the second-order crystallographic axis. The obtained values of TPA coefficients are higher than for BiBO crystals that were also investigated by us.

1. Introduction

Owing to possible 3- or 4-fold coordination of boron atoms, borates form a great number of compounds having diverse structures. Many of them show superior nonlinear optical properties (NLO) compared to the well known inorganic compounds [1]. These borates in form of single crystals find numerous applications in laser and NLO applications. Especially, borate crystals play important role in UV applications due to their relatively high UV transparency, good NLO efficiency and high damage threshold for laser radiation. The borate family have been widely studied in last years and as a result several new promising materials have been found, namely $CsLiB_6O_{10}$ (CLBO) [2], $Ca_4ReO(BO_3)_3$, Re = Gd, Y (ReCOB)

*Author to whom all correspondence should be addressed.
0022-2461
DOI: 10.1007/s10853-006-4487-5

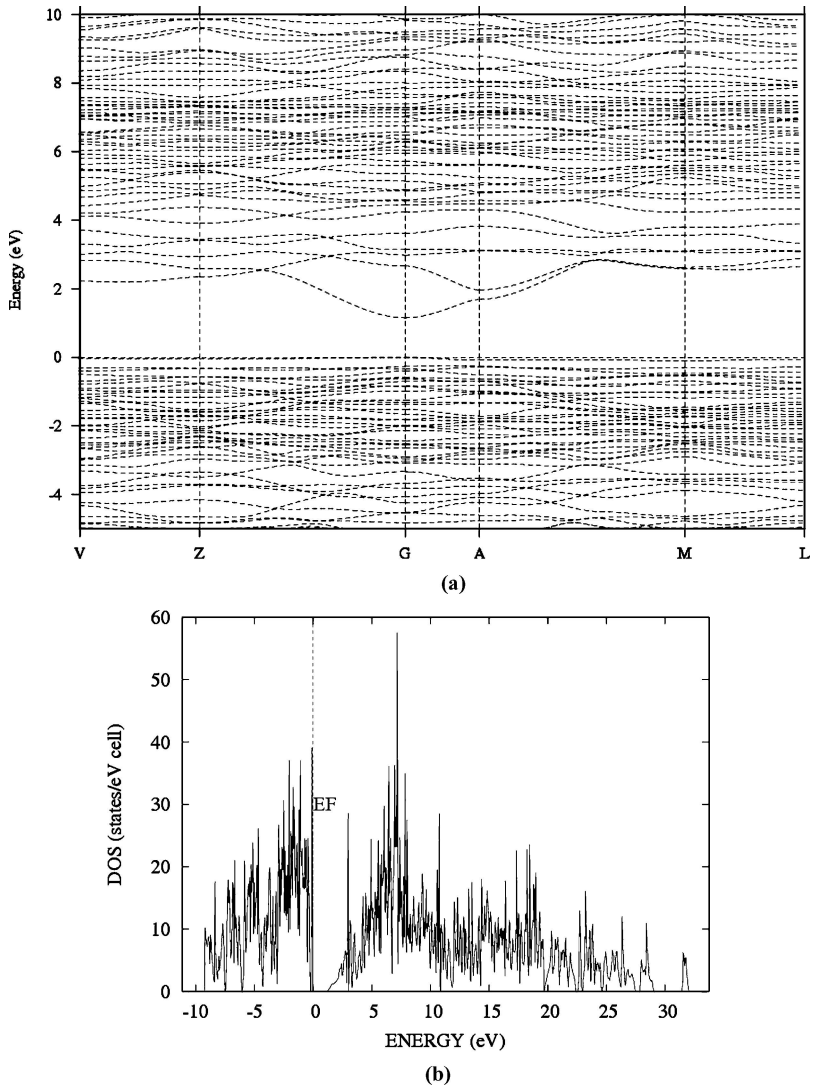

Figure 1 a) Band energy dispersion of the LCB crystals. b) Density of state (states/eV cell) for the investigated crystal.

and BiB_3O_6 (BiBO) [3–6]. These crystals allow efficient generation of radiation in UV and visible region due to higher harmonics generation of external laser sources or self-frequency doubling (SFD) when a crystal acts simultaneously as a laser and NLO material. One of new borate crystals showing NLO properties is lanthanum calcium borate $La_2CaB_{10}O_{19}$ (LCB) discovered by Wu *et al*. [7]. The material crystallizes in a centric structure (monoclinic, space group C2). It has slightly higher birefringence than YCOB (0.053, and 0.041 at 1064 nm, respectively), what allows to perform second harmonic generation (SHG) in this material down up to 288 nm, compared to 360 nm in case of YCOB [8]. La^{3+} ions in this crystal provide sites for Nd^{3+} [9] or Yb^{3+} [10] substituting. As a result a multifunctional material showing SFD properties may be synthesized. Moreover, according to Wang *et al*. [11] its d_{eff} (1.05 pm/V, $\lambda = 1.06\ \mu$m) is larger than that for LiB_3O_5 (LBO) and KH_2PO_4 (KDP), LCB is insensitive to moisture in contrary to LBO, KDP, and β-BaB_2O_4 (BBO), and the damage threshold is higher than that of BBO and $KTiOPO_4$ (KTP). All these features make LCB crystals a good candidate for SHG conversion applications. In this paper we describe investigations of UV-induced two-photon absorption in LCB crystals.

2. Experimental

2.1. $La_2CaB_{10}O_{19}$ crystal growth

According to the phase diagram given by Wu *et al*. [8] LCB melts incongruently, so high temperature solution growth should be used to obtain it in a form of single crystal. According to Wang *et al*. [12] Czochralski growth of LCB crystals from stoichiometric melts is also possible due to small difference in melting temperature and peritectic phase transition temperature of LCB, however such a crystallization is disturbed by crystallization of lanthanum borate LaB_3O_6 at the bottom of the crucible. The phase diagram of the system LaB_3O_6-CaB_4O_7 shows that in the broad range of composition, when an excess of CaB_4O_7 is used, monoclinic LCB phase is the only crystallizing phase [8].

In our experiments an excess of CaB_4O_7 was used as a solvent. The synthesis of the starting material was carried

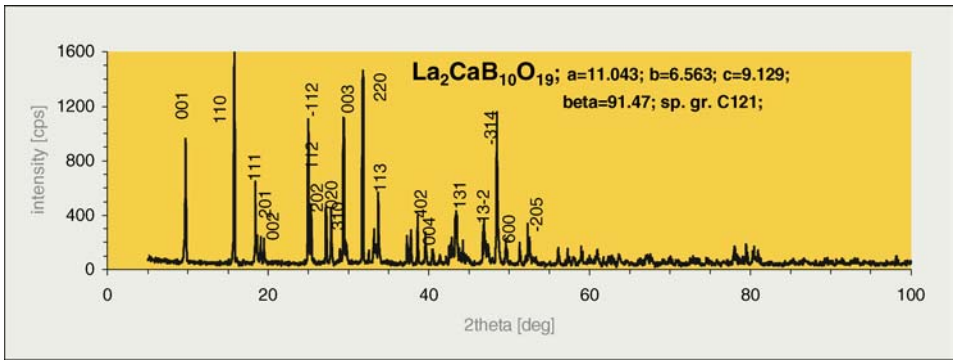

Figure 2 X-ray powder diffraction pattern of LCB crystals.

out under strict control to avoid changes in composition of the melt caused by evaporation of CaB_4O_7. Wu *et al.* [8] carried out the LCB crystallization from melts containing 30 mol% excess of calcium tetraborate comparing the stoichiometric composition. Our investigations suggest that 30 mol% excess of CaB_4O_7 may be not sufficient because of strong evaporation of the solvent that could shift the composition of the melt to the area of LaB_3O_6 crystallization. We used near 60 mol% of CaB_4O_7 in LaB_3O_6-CaB_4O_7 system given in [8]. Two-zone resistance furnace was used to crystallize LCB from a platinum crucible. The lower zone secured the proper temperature of the melt, while the upper zone was used to diminish the temperature gradients in the crystallization region, what is a necessary condition during high temperature solution growth. The details of the crystallization set can be found elsewhere [13]. Recrystallized rods of LCB glass were used as seeds during processes of top seeded solution growth (TSSG). Due to polycrystalline structure of these seeds LCB crystallized in form of numerous plates having average dimensions of $3\times3\times1$ mm, which were used in our investigations. In Fig. 2 there is shown a powder X-ray diffraction pattern confirming monoclinic structure of the obtained crystals (a = 11.043 Å, B = 6.563 Å, c = 9.129 Å, $\beta = 91.47^\circ$). The obtained crystals will be used in future experiments as seeds to obtain more bulky LCB single crystals.

3. Third-order optical properties of LCB

3.1. General formalism of two-photon absorption

The LCB crystals also may be of interest because of the third-order optical applications, particularly for the two-photon absorption (TPA) described by the imaginary part of fourth rank optical susceptibility tensors. Nonlinear optical effects are generally described phenomenologically by the optical response P, of a material to an effective electric field, $\vec{E}$ [14]:

$$P_i(\vec{r},t) = \chi_{ij}^{<1>} \cdot E_j(\vec{r},t) + \chi_{ijk}^{<2>} \cdot E_j E_k(\vec{r},t) + \chi_{ijkl}^{<3>} \cdot E_j E_k E_l(\vec{r},t) + \ldots \quad (1)$$

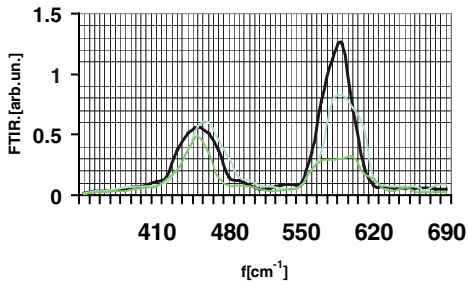

Figure 3 Changes of the FTIR spectra versus different UV-induced power densities: green -0.1 GW/cm^2; blue -0.4 GW/cm^2 ; black -0.8 GW/cm^2.

The $\chi_{ij}^{<1>}$ term is responsible here for linear optics phenomena like light reflection and refraction. The $\chi_{ij}^{<2>}$ terms and $\chi_{ijkl}^{<3>}$ are responsible for nonlinear optical phenomena and correspond to the second- and third-order optical effects, respectively. The Ek, El are effective electric strength field components.

When the charges in a material are bound by a harmonic potential, the induced dipole moment is linear to the applied electric field $\vec{E}$. The response of a molecule is 'nonlinear' if the charges are bound to the molecule by a anharmonic potential. In this case, the dipole moment of the molecule is a nonlinear function of applied electric field strength. More generally, if a 'nonlinear' molecule is exposed to light, the time-dependent induced dipole moment is a nonlinear function of the time-dependent electric field $\vec{E}$. For a slowly varying electric field, the induced molecular dipole moment and corresponding polarizability, P can be expanded as a power series versus the applied electric field $\vec{E}$ [15]:

$$P_i(\vec{r},t) = P_l^{(0)} + \alpha_{ij} \cdot E_j(\vec{r},t) + \beta_{ijk} \cdot E_j E_k(\vec{r},t) + \gamma_{ijkl} \cdot E_j E_k E_l(\vec{r},t) + \ldots \quad (2)$$

where the subscripts refer to the Cartesian vector or tensor components of each quantity $P_l^{(0)}$, is the i-th component of the crystal's static dipole moment, α_{ij} is the linear microscopic polarizability, β_{ijk} and γ_{ijk} correspond to second- and third-order susceptibilities, respectively.

Generally the TPA does not require a charge density non-centrosymmetry. However it is determined by dipole moments both of ground as well as of excited states. To create additional possibilities of their using as third-order optical materials it is necessary to create substantial enhancement of corresponding dipole moments.

One can clearly see substantial enhancement of the anharmonic phonon modes during increasing of the UV-induced power (see Fig. 3), contrary to the usual harmonic mode at about 585 nm. The phonon modes situated at lower frequencies (for example at 450 nm) are almost not sensitive to the UV-induction. So this fact indicates on occurrence of the photoinduced anharmonic modes within the bulk crystals propagating from the thin UV-induced layers through the crystal.

4. Theoretical calculations

We have performed *ab initio* calculations for the monoclinic semiconducting $La_2CaB_{10}O_{19}$ crystal. The space group is $C2$ with $a = 11.043(3)$ Å, $b = 6.563(2)$ Å, $c = 9.129(2)$ Å, $\alpha = \gamma = 90^\circ$, $\beta = 91.47^\circ$ [17], and two formula units per cell. The crystal structure contains B_5O_{12} double-ring pentaborate groups, which are linked together to form an infinite two-dimensional double layer. The layer runs almost perpendicular to the **c**-axis of the crystal. The La atoms are located in layers, while the Ca atoms are located between two layers. $La_2CaB_{10}O_{19}$ exhibits an optical second-harmonic generation effect about twice as large as that of KDP (KH_2PO_4). In our calculations we used the first-principle self-consistant, tight-binding, linear muffin-tin orbital (TB-LMTO) of Anderson and Jepsen [18] method. The von Barth-Hedin [19] parameterization is used for the exchange correlation potential within the local density approximation. In the present calculation, we used the atomic sphere approximation. In addition to 36 empty sheres we include corrections for neglect of interstitial regions and primary waves of higher order. The Brillouin zone $\vec{k}$-points integrations are made using the tetrahedron method on a grid of 136 $\vec{k}$-points in the irreducible Brillioun zone (IBZ) to obtain converged results.

4.1. The principal parameters of the band structure and density of states

Fig. 1 shows the band energy dispersion and the density of states (DOS) of the investigated LCB crystals calculated by using TB-LMTO. From Fig. 1a one can see that the valence band and conduction band have substantially different band energy dispersion, which corresponds to substantially different mobilities between the localized holes and delocalized non-occupied semiconducting bands. Such situation is extremely effective for different kinds of photoinduced effects due to excitation of the localized excitons to the delocalized states. At the same time the hyperpolarizabilities should be also maximal for these bands due to the substantially different values of effective masses within the 2–6 eV. With the further increase of the values the effect should be suppressed due to the higher localization of the band structure. The more effective pumping may be observed near the G and Z symmetry points of the BZ. We note that the valence band maximum (VBM) is located at Z and the conduction band minimum (CBM) at G resulting in an indirect energy gap of 1.5 eV.

The similar situation is observed from the DOS (see Fig. 1b) which unambiguously show that the effect will be maximal for the wavelengths about 215 nm. So we should use those wavelengths for the pumping and the maximal gradient should be observed at the 2, 4 eV, so these wavelengths should be used for the probing beams.

5. TPA set-up

We have performed measurements of photoinduced TPA using as a source laser beam generation of the Raman shifted Nd-YAG laser with $\lambda = 1.9$ μm with pulse duration 20 ps, frequency repetition 11 Hz and maximal peak power about 22 MW. At the same time we have used the second and fourth harmonics of this laser with wavelengths 0.95 and 0.475 μm, respectively.

Principal experimental set-up for the performing of the photoinduced TPA is shown in Fig. 4. The polarized light from the excimer laser ($\lambda = 217$ nm) creates strong electric strength in thin nano-layer of LCB crystal. The system of polarisers and mirrors allows to achieve the angle between the pumping UV-inducing polarized light beam and the fundamental one about $10\text{-}12^0$. The registration system consisting from the photomutiplier together with the electronic boxcar registration system allows monitoring the kinetics of the output transparency versus intensity power of the probing laser beams.

Because the thickness of the UV-induced layer is equal about 85 nm due to the LBC absorption coefficient 2×10^4 cm^{-1} the effective 85 nm thick layer becomes a source generating anharmonic phonon modes propagating into the bulk crystal and creating charge density non-centrosymmetry. Varying polarization of the incident and output beams we are able to analyze different tensor components of the optical susceptibility corresponding to the TPA.

The TPA coefficient was evaluated with precision of about 0.3 cm/GW from intensity-dependent transparency T using an expression:

$$T = 1 - \beta d I \tag{3}$$

Here d- is sample's thickness; I - intensity of fundamental beam; β- two-photon absorption coefficient. For reliable control we have done all the measurements at different sample's thickness and at varying angles between directions of polarization between pump UV light and probe IR laser beams. In order to investigate the pump

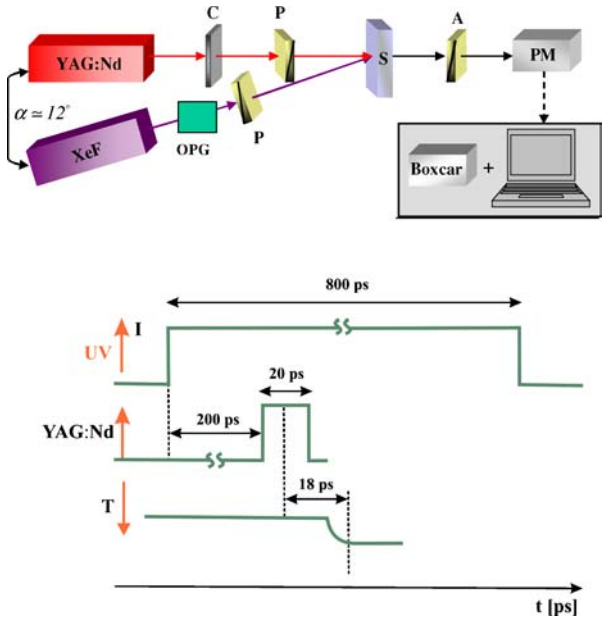

Figure 4 Principal schema of experimental set-up.

wavelength dependences additional optical parametrical generator (**OPG**) was used.

5.1. Results of the TPA measurements and discussion

Typical measured intensity-dependent transparencies for pumping wavelength 217 nm are shown in Fig. 5. One can see an occurrence of a bending in the corresponding transparency versus UV-induced intensities. Increasing of the UV-pump power leads to the increasing values of the TPA coefficients. Shifting the beginning of the probing beam with respect to the time of achievement of maximum for the probe beam we have revealed that the transparency achieves its saturation at about 20 ps with delay about 230 ps after the starting of the pump pulse. So one can see that photoinduced absorption kinetics is saturated. Crucial role also may be played here by a competition between formation of electron-phonon anharmonic polarization and free carrier diffusion due to the defects presence.

The performed investigations have shown that maximal TPA coefficient β is achieved for parallel polarizations of the pumping (using excimer Xe-F laser with $\lambda = 0.217\mu$m, time duration about 0.8 ns) and probing beams, and delaying time between the pumping and probing laser beams equal to 20 ps. The best results were achieved for the polarization of the pump light directed along the second-order optical axis, corresponding to the χ_{2222} tensor component. This fact reflects substantial role played by the anharmonic electron-phonon interactions to the mentioned third-order optical susceptibilities. One can expect that the thin UV-induced layer is a source of anharmonic phonon fluence responsible for the observed TPA. Varying the samples' thickness within the

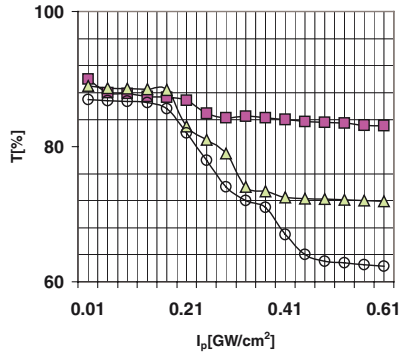

Figure 5 Typical dependences of the transparency versus fundamental power density: □ - without UV-pumping; Δ - for the UV-photoinduced power about 0.5 GW/cm^2; ○ - for the 0.75 GW/cm^2. All the measurements are done for the pump-probe delaying time about 18 ps.

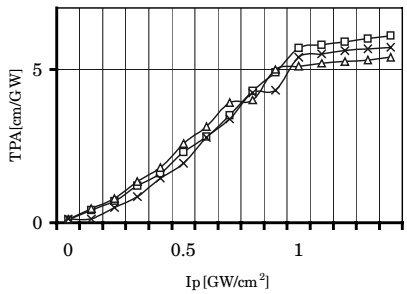

Figure 6 Dependence of the UV-induced TPA versus the pump power density for different probing wavelengths: □ - 475 nm; X - 950 nm; Δ - 1900 nm.

0.07–0.4 mm we have established that the effect is similar to the bulk-like one. Because the free carriers are not able to penetrate more than 85 nm one can expect a crucial role played by electrostricted phonons propagating through the sample.

From Fig. 6 one can see that at pumping UV excimer laser beam power densities about 1.1 GW/cm^2 there appears a saturation of the TPA coefficient. This also may reflect a possibility of inclusion the cascading nonlinear optical processes of higher order. The values of the obtained TPA coefficients indicate on possibility of using the mentioned crystals as optically operated limiters in a wide spectral range. Changes of sample thickness do not change substantially the features of the TPA confirming the bulk-like origin of the phenomenon with the nanolayer source.

Following the performed band energy calculations presented above we have done additional measurements with the other wavelength. From the Fig. 7 one can clearly see that the increasing pumping wavelength leads to a suppression of the TPA signal (up to 0.9 cm/GW) at 420 nm. This is in an agreement with the calculated band structure presented in the Fig. 1. From Fig. 8 one can clearly see that with increase of the pump power density we observe enhanced TPA values.

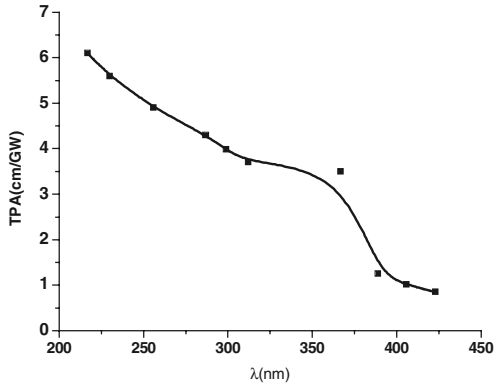

Figure 7 Dependence of the TPA versus the pumping wavelength.

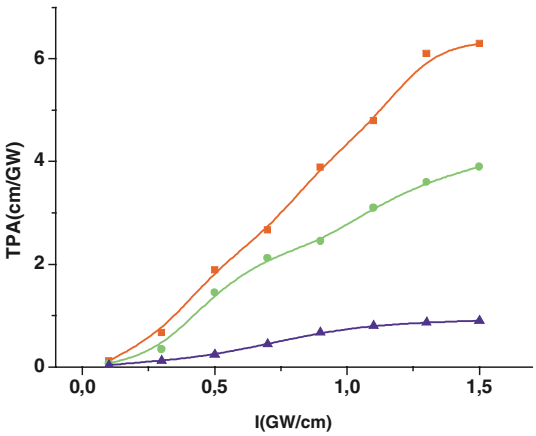

Figure 8 Dependences of the TPA versus power densities of the pumping waves possessing different wavelengths: traingles 420 nm; rings - 380 nm; squares - 217 nm.

6. Conclusions

In this paper we show that LCB crystals may be of interest due to the UV-operated TPA. We performed photoinduced TPA measurements using excimer Xe-F laser ($\lambda = 217$ nm) as a source of the photoinducing beam and for the longer wavelengths. The illumination created a thin near-the-surface layer (85 nm) in which photoinduced TPA within the bulk volume was observed. The Raman shifted Nd-YAG laser radiation ($\lambda = 1.9\mu$m) as well as its second and fourth harmonics ($\lambda = 950$ and $\lambda = 475$ nm, respectively) were used as fundamental beams. It is important that the using of the higher wavelength leads to substantial suppression of the TPA, which is confirmed by the band energy structure calculations.

The highest values of the TPA β coefficient were achieved for the polarization of the pumping light directed along the second-order optical axis. The obtained values of the TPA coefficients indicate on a possibility of using LCB crystals as optically-operated limiters in the wide spectral range. The performed quantum chemical simulations and Raman spectra confirm substantial role played by UV-induced electron-phonon anharmonicity in the observed effects. Their efficiency is at least 3 times higher than in case of BiBO crystals [16]. In order to make more detailed comparison with the experimental data, we have performed calculations of the band energy dispersion and DOS for LCB crystal using LMTO method. Our results for band energy dispersion and DOS show that this crystal is a semiconductor with small indirect energy gap of 1.5 eV.

Acknowledgments

This work was partly supported by the Polish Committee for Scientific Research, Grants No 1 P03B 058 27 and 4 T11B 051 25. We would like to thank Prof. O. K. Andersen for using the TB-LMTO code.

References

1. C. CHEN, Y. WU and R. LI, *J. Cryst. Growth* **99** (1990) 790.
2. Y. MORI, I. KURODA, T. SASAKI and S. NAKAI, *Jpn. J. Appl. Phys.* **34** (1995) L296.
3. G. AKA, A. KHAN-HARARI, D. VIVIEN, J.M. BENITEZ, F. SALIN and J. GODARD, *Eur. J. Solid State Inorg. Chem* **33** (1996) 727.
4. T. LUKASIEWICZ, I. V. KITYK, M. MAKOWSKA-JANUSIK, A. MAJCHROWSKI, Z. GALAZKA, H. KADDOURI and Z. MIERCZYK, *J. Cryst. Growth* **237–239** (2002) 641.
5. H. HELLWIG, J. LIEBERTZ and L. BOHATY, *Solid State Commun.* **109** (4) (1999) 249.
6. M. GHOTBI, M. EBRAHIM-ZADEH, A. MAJCHROWSKI, E. MICHALSKI and I. V. KITYK, *Optics Letters* **29** (2004) 2530.
7. Y. WU, J. LIU, P. FU, J. WANG, F. GUO, G. ZHAO, J. QIN and C. CHEN, *Proc. SPIE* **3556** (1998) 8.
8. YICHENG WU, PEIZHEN FU, FENG ZHENG, SONGMING WAN and XIANGGUO GUAN, *Optical Materials* **23** (2003) 373.
9. PEIZHEN FU, JUNXIN WANG, HAIQUAN GUO, HENGLI ZHANG, ZUYAN XU, FAN GUO and YICHENG WU, *Progress in Crystal Growth and Characterization of Materials*, (2000) 107.
10. PEIZHEN FU, FANGLI JING, FENG ZHENG and YICHENG WU, *Journal of the Chinese Ceramic Society* **32**(3) (2004) 245.
11. GUILING WANG, JUNHUA LU, DAFU CUI, ZUYAN XU, YICHENG WU, PEIZHEN FU, XIANGGUO GUAN and CHUANGTIAN CHEN, *Optics Communications* **209** (2002) 481.
12. JUNXIN WANG, PEIZHEN FU and YICHENG WU, *J. Cryst. Growth* **235** (2002) 5.
13. A. MAJCHROWSKI, M. T. BOROWIEC and E. MICHALSKI, *J. Cryst. Growth* **264** (2004) 201.
14. R. W. BOYD, Nonlinear optics, Academic Press, 1992.
15. C. MARTINEAU, G. LEMERCIER and C. ANDRAUD, *Optical Materials* **21** (2002) 555.
16. A. MAJCHROWSKI, J. KISIELEWSKI, E. MICHALSKI, K. OZGA, I. V. KITYK and T. LUKASIEWICZ, *Opt. Com.*, in print, doi: 10.1016/j.optcom.2005.02.053.
17. YICHENG WU, JIANGUO LIU, PEIZHEN FU, JUNXING WANG, HUYUN ZHOU, GUOFU WANG and CHUANGTIAN CHEN, *Chem. Mater.* **13**(3) (2001) 753.
18. O. K. ANDERSEN and O. JEPSEN, *Phys. Rev. Lett.* **53** (1984) 2571.
19. U. VON BARTH and L. HEDIN, *J. Phys. C* **5** (1972) 1629.

Received 8 March
and accepted 21 June 2005